

This is the final version of the following paper published by Journal of Applied Physics:

H. Rahbardar Mojaver, Farzin Manouchehri, and Pouya Valizadeh, “Theoretical Evaluation of 2DEG Characteristics of Quaternary $\text{Al}_x\text{In}_y\text{Ga}_{1-x-y}\text{N}/\text{GaN}$ Hetero-junctions”, Journal of Applied Physics, vol. 119, no. 15, pp. 154502-1–154502-7, Apr. 2016.

doi: 10.1063/1.4946842

AIP Publishing grants to the author(s) the right to post their accepted manuscript anywhere on the web immediately after acceptance by the Journal. In addition, 12 months after publication, the final AIP Publishing version may be posted on the author's personal website, the author's institutional website, or in an institutional or funder-designated repository. It is also possible to create a link to the Journal of Applied Physics publication.

Theoretical evaluation of two dimensional electron gas characteristics of quaternary $\text{Al}_x\text{In}_y\text{Ga}_{1-x-y}\text{N}/\text{GaN}$ hetero-junctions

Hassan Rahbardar Mojaver, Farzin Manouchehri, and Pouya Valizadeh

Citation: *Journal of Applied Physics* **119**, 154502 (2016); doi: 10.1063/1.4946842

View online: <https://doi.org/10.1063/1.4946842>

View Table of Contents: <http://aip.scitation.org/toc/jap/119/15>

Published by the *American Institute of Physics*

Articles you may be interested in

[Two dimensional electron gases induced by spontaneous and piezoelectric polarization in undoped and doped AlGaN/GaN heterostructures](#)

Journal of Applied Physics **87**, 334 (2000); 10.1063/1.371866

[Use of a bilayer lattice-matched AlInGaN barrier for improving the channel carrier confinement of enhancement-mode AlInGaN/GaN hetero-structure field-effect transistors](#)

Journal of Applied Physics **121**, 244502 (2017); 10.1063/1.4989836

[Two-dimensional electron gases induced by spontaneous and piezoelectric polarization charges in N- and Ga-face AlGaN/GaN heterostructures](#)

Journal of Applied Physics **85**, 3222 (1999); 10.1063/1.369664

[Dielectric function and optical properties of quaternary AlInGaN alloys](#)

Journal of Applied Physics **110**, 013102 (2011); 10.1063/1.3603015

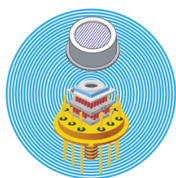
[Investigation of gate leakage current mechanism in AlGaN/GaN high-electron-mobility transistors with sputtered TiN](#)

Journal of Applied Physics **121**, 044504 (2017); 10.1063/1.4974959

[Compositional variation of nearly lattice-matched InAlGaN alloys for high electron mobility transistors](#)

Applied Physics Letters **96**, 252108 (2010); 10.1063/1.3456561

Ultra High Performance SDD Detectors



See all our XRF Solutions

Theoretical evaluation of two dimensional electron gas characteristics of quaternary $\text{Al}_x\text{In}_y\text{Ga}_{1-x-y}\text{N}/\text{GaN}$ hetero-junctions

Hassan Rahbardar Mojaver, Farzin Manouchehri, and Pouya Valizadeh^{a)}

Department of Electrical and Computer Engineering, Concordia University, Montreal, Quebec H3G-1M8, Canada

(Received 4 January 2016; accepted 3 April 2016; published online 18 April 2016)

The two dimensional electron gas (2DEG) characteristics of gated metal-face wurtzite $\text{AlInGaN}/\text{GaN}$ hetero-junctions including positions of subband energy levels, fermi energy level, and the 2DEG concentration as functions of physical and compositional properties of the hetero-junction (i.e., barrier thickness and metal mole-fractions) are theoretically evaluated using the variational method. The calculated values of the 2DEG concentration are in good agreement with the sparsely available experimental data reported in the literature. According to our simulation results, a considerable shift in the positive direction of threshold voltage of $\text{AlInGaN}/\text{GaN}$ hetero-junction field-effect transistors can be achieved by engineering both the spontaneous and the piezoelectric polarizations using a quaternary AlInGaN barrier-layer of appropriate mole-fractions. *Published by AIP Publishing.*
[\[http://dx.doi.org/10.1063/1.4946842\]](http://dx.doi.org/10.1063/1.4946842)

I. INTRODUCTION

Over the past two decades, III-nitride hetero-junction field-effect transistors (HFETs) have attracted a great deal of attention for fulfilling the growing demands in high-power mm-wave and high-voltage power-electronic applications.^{1,2} Among III-nitride devices, $\text{AlGaIn}/\text{GaInN}$ HFETs have managed to offer power densities as high as 40 W/mm at 4 GHz,³ 10 W/mm at 40 GHz,⁴ maximum oscillation frequencies over 300 GHz,⁵ current densities in excess of 1 A/mm, and breakdown voltages exceeding 2000 V.⁶ These attractive figures of merit of RF power amplification and power switching are direct results of a number of superior device/material properties, including large sheet carrier concentration (i.e., in the order of 10^{13} cm^{-2}) and high breakdown fields (i.e., about 4 MV/cm). The large sheet carrier concentration at these hetero-interfaces produces the normally on HFET characteristic. Hence, the realization of normally off devices, which is necessary for efficient power management, single polarity power supply circuits, and safer switching in power switching applications, has proven difficult. In addition to the power switching applications, based on the observations made in a few other compound semiconductor technologies on the importance of normally off devices in improving the noise figure,⁷ normally off III-nitride HFETs have also generated interest for RF applications.

Several different approaches have been proposed to realize normally off GaN HFETs.⁸⁻¹⁷ One of the more promising methods is based on employing a quaternary $\text{Al}_x\text{In}_y\text{Ga}_{1-x-y}\text{N}$ barrier-layer,¹²⁻¹⁷ using which normally off characteristic with a threshold voltage of 0.56 V has been reported.¹⁷ Depending on the Al and In mole-fractions (x and y) of this barrier-layer, pseudomorphic growth of the $\text{AlInGaIn}/\text{GaInN}$ hetero-junction is capable of developing both tensile and

compressive strain at the hetero-interface. In addition, the discontinuity of the spontaneous polarization at the hetero-interface can be controlled by these mole-fractions. Since the concentration of the two dimensional electron gas (2DEG) formed at III-nitride hetero-junctions is predominantly defined via the piezoelectric and the spontaneous polarizations, changing the group-III metal mole-fractions in the barrier can be used as an effective tool in engineering the threshold voltage of HFETs realized on these hetero-junctions.

Thus far, only a few investigations that include theoretical study of the 2DEG characteristics of $\text{AlInGaIn}/\text{GaInN}$ hetero-junctions have been presented.^{13,14} However, determination of fermi and subband energy levels at the quaternary hetero-interface quantum well, which is essential for the calculation of 2DEG concentration, has not been discussed in the aforementioned studies. Moreover, providing a reliable evaluation basis for the 2DEG characteristics as functions of physical and compositional properties of the quaternary hetero-junctions has been so far overlooked. This paper aims to fulfill the need for a more accurate theoretical evaluation of the 2DEG characteristics of $\text{AlInGaIn}/\text{GaInN}$ hetero-junctions. This includes explaining the trends between the threshold voltage and physical/compositional properties of the barrier.

The basis of the theoretical model is presented in Section II. Section III presents the results and discussion. Section III is followed by concluding remarks.

II. THEORETICAL MODELING

Details of the theoretical model exploited in this study have been previously reported in Ref. 18. The studied hetero-structures are composed of a thin AlInGaIn barrier layer grown pseudomorphically on top of a thick GaN channel/buffer layer, where Ni established a Schottky contact to AlInGaIn . In adopting this theoretical model, which was originally developed for $\text{AlGaIn}/\text{GaInN}$ hetero-junctions, to

^{a)}Electronic mail: p.valizadeh@ieec.org.

AlInGa_xN/GaN quaternary hetero-junctions, appropriate values of polarization induced charges at the hetero-interface, conduction band discontinuity, and Schottky barrier height are recalculated. The details of these calculations are presented in the Secs. II A–II C.

A. Hetero-interface polarization induced charge

Considering the nonlinear variations of piezoelectric polarization of Wurtzite III-nitride semiconductors with respect to metal mole-fractions, Vegard's law can be employed in evaluating the piezo-electric polarization of a polar Al_xIn_yGa_{1-x-y}N/GaN epilayer¹⁹

$$P_{PZ}(\text{Al}_x\text{In}_y\text{Ga}_{1-x-y}\text{N}) = xP_{PZ}(\text{AlN}) + yP_{PZ}(\text{InN}) + (1-x-y)P_{PZ}(\text{GaN}), \quad (1)$$

where x and y are Al and In mole-fractions, and P_{PZ} for binaries are nonlinear functions of basal strain (μ) between Al_xIn_yGa_{1-x-y}N and GaN layers.

In order to calculate the spontaneous polarization of the quaternary AlInGa_xN barrier-layer, Vegard's law with the incorporation of the associated nonlinearities is adopted according to Ref. 19. The spontaneous polarization can be therefore calculated as

$$P_{SP}(\text{Al}_x\text{In}_y\text{Ga}_{1-x-y}\text{N}) = xP_{SP}(\text{AlN}) + yP_{SP}(\text{InN}) + (1-x-y)P_{SP}(\text{GaN}) + b_{SP}^{\text{AlGaN}}x(1-x-y) + b_{SP}^{\text{InGaN}}y(1-x-y) + b_{SP}^{\text{AlInN}}xy, \quad (2)$$

where b_{SP}^{AlGaN} , b_{SP}^{InGaN} , and b_{SP}^{AlInN} are the bowing parameters of ternaries AlGa_xN, InGa_xN, and AlIn_xN, respectively. The values of the parameters used in calculating the piezoelectric and spontaneous polarization are presented in Table I.

The total polarization vector of a metal-face wurtzite III-nitride AlInGa_xN/GaN hetero-junction not disturbed by any external force is calculated by the summation of spontaneous and piezoelectric polarizations. Additionally, the polarization-induced charge density is the result of the divergence of the polarization along the growth direction.

TABLE I. Parameters used for the calculation of piezoelectric and spontaneous polarization in AlInGa_xN epilayer.¹⁹

Parameter	Value (C/m ²)
$P_{PZ}(\text{AlN})$	$-1.808 \times \mu - 7.888 \times \mu^2$ for $\mu > 0$ $-1.808 \times \mu + 5.624 \times \mu^2$ for $\mu < 0$
$P_{PZ}(\text{InN})$	$-1.373 \times \mu + 7.559 \times \mu^2$
$P_{PZ}(\text{GaN})$	$-0.918 \times \mu + 9.541 \times \mu^2$
$P_{SP}(\text{AlN})$	-0.0898
$P_{SP}(\text{InN})$	-0.0413
$P_{SP}(\text{GaN})$	-0.0339
b_{SP}^{AlGaN}	0.0191
b_{SP}^{InGaN}	0.0378
b_{SP}^{AlInN}	0.0709

Therefore, the two dimensional charge density at the metal-face hetero-interface is equal to

$$\begin{aligned} \sigma &= \Delta P_{SP} + \Delta P_{PE} \\ &= [P_{SP}(\text{AlInGaN}) - P_{SP}(\text{GaN})] \\ &\quad + [P_{PZ}(\text{AlInGaN}) - P_{PZ}(\text{GaN})], \end{aligned} \quad (3)$$

where ΔP_{SP} and ΔP_{PZ} are the difference in spontaneous and piezoelectric polarizations between the barrier and buffer/channel layer. In order to evaluate the predictive power of the present model, Table II presents a comparison between the results obtained through Eqs. (1)–(3) and the limited experimental data reported in the literature.

Figure 1 presents the bandgap versus lattice constant of Al_xIn_yGa_{1-x-y}N for all possible values of x and y with indication of ΔP_{SP} equi-contours (a), ΔP_{PZ} equi-contours (b), and sheet charge density equi-contours (c) at Al_xIn_yGa_{1-x-y}N/GaN hetero-interface with corresponding values of x and y . The bandgap of the quaternary AlInGa_xN is estimated using Vegard's law by employing the ternary alloy bowing parameters according to the following equation:²¹

$$\begin{aligned} E_G(\text{AlInGaN}) &= (1-x-y)E_G(\text{GaN}) + xE_G(\text{AlN}) \\ &\quad + yE_G(\text{InN}) - b_{EG}^{\text{AlGaN}}x(1-x) \\ &\quad - b_{EG}^{\text{InGaN}}y(1-y) \\ &\quad - (b_{EG}^{\text{AlInN}} - b_{EG}^{\text{AlGaN}} - b_{EG}^{\text{InGaN}})xy. \end{aligned} \quad (4)$$

The values used for the bandgap of binary end-points and ternary bowing parameters are presented in Table III. It should be noted that the bandgap-related bowing parameters of III-nitrides are still under investigation.^{21–23} Regarding Fig. 1(a), the contours show approximately similar value of spontaneous polarization for the layers with identical value of Al mole-fraction. This is because the high spontaneous polarization of AlN in comparison with GaN and InN makes the spontaneous polarization of AlInGa_xN to depend mainly on the Al mole-fraction. However, according to Fig. 1(b), for moderate values of x and y , contours of piezo-electric polarization are defined almost vertically, which confirms the dependence of piezo-electric polarization on basal strain and consequently lattice constant of the AlInGa_xN layer.

Figure 1(c) illustrates the total polarization-induced sheet charge density at the hetero-interface. As previously mentioned, the quaternary barrier-layer provides us with the capability of engineering both the bandgap and the total polarization effect at the hetero-interface. In this figure, the

TABLE II. Polarization-induced sheet charge density (σ) at Al_{0.54}In_{0.12}Ga_{0.34}N/GaN hetero-interface calculated based on the model expressed by (1)–(3) and the sparsely available experimental data. The experimental data are provided in Ref. 20.

σ ($\mu\text{C}/\text{cm}^2$)	Method
2.14	Model expressed by (1)–(3)
2.099 ± 0.054	Hall measurement
1.978 ± 0.036	I _D -V _G measurement
1.968 ± 0.133	C-V measurement

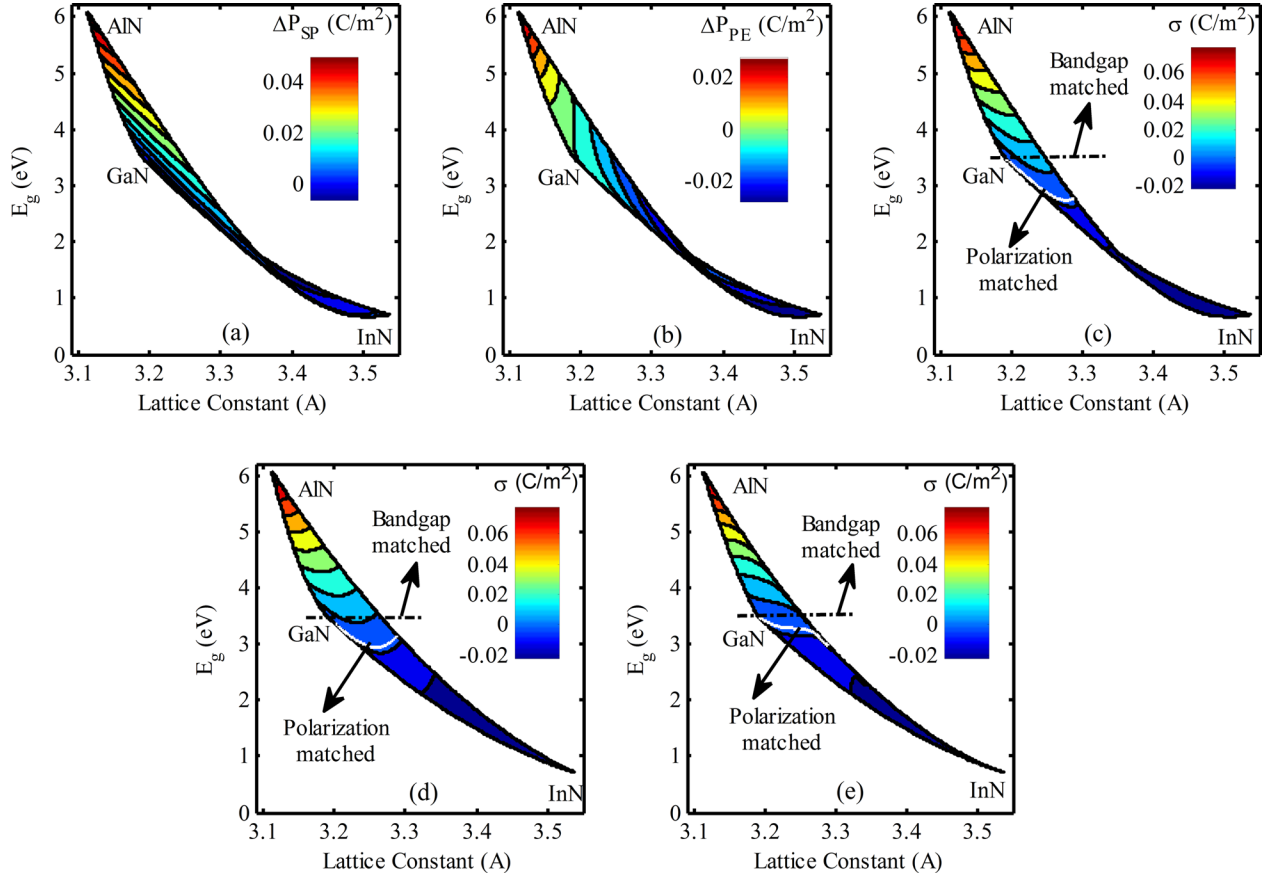


FIG. 1. Bandgap vs. lattice constant for $\text{Al}_x\text{In}_y\text{Ga}_{1-x-y}\text{N}$ quaternary barrier-layer with indication of ΔP_{SP} equi-contours (a), ΔP_{PZ} equi-contours (b), and sheet charge density equi-contours (c) at $\text{Al}_x\text{In}_y\text{Ga}_{1-x-y}\text{N}/\text{GaN}$ hetero-interface for the corresponding values of x and y . (d) and (e) represent plots identical to (c) if the bandgap is calculated using the bowing parameters presented in Refs. 22 and 23, respectively.

corresponding contour for which the sheet charge density is equal to zero is indicated. The corresponding border at which the bandgap of the barrier and buffer/channel layer are matched is also highlighted. Based on the results depicted in Fig. 1(c), an interesting observation is that, contrary to the previously claimed possibility of offering polarization-matched quaternary hetero-junctions while retaining the large bandgap of the barrier-layer and the resulting proper carrier confinement,^{13,17,24} this structure is not capable of implementing this twofold characteristic simultaneously. In other words, as evident from Fig. 1(c), for a polarization-matched barrier-layer, the buffer/channel layer exhibits a larger bandgap that rules out the possibility of developing a quantum-well at the hetero-interface. Therefore, no carrier confinement exists in this condition. Although exact

matching of polarization is not possible, quaternary barriers can still help design devices with low interface polarization charge. Figures 1(d) and 1(e) show the total polarization-induced sheet charge density if the bandgap of the barrier is calculated using the bowing parameters presented in Refs. 22 and 23, respectively. These figures confirm that independent of the choice of reference for the bowing parameters, a similar observation on the inability of polarization-matched barriers to produce a positive conduction band discontinuity is made.

B. Conduction band discontinuity

Thus far, there has been little work dedicated to evaluation of conduction band discontinuity (ΔE_C) of III-nitride quaternary $\text{AlInGaN}/\text{GaN}$ hetero-junctions. According to Ref. 25, ΔE_C is evaluated as the difference between the discontinuity of the bandgap and that of the valence band (i.e., ΔE_V). The ratios of $\Delta E_C/\Delta E_V$ for AlN/GaN , GaN/InN , and AlN/InN are reported as 70:30, 60:40, and 70:30, respectively.²⁶

A framework according to Vegard's law was adopted by Satpathy *et al.*²⁷ for calculation of ΔE_V of ternary AlGaIn/GaN hetero-junctions. However, lack of existing knowledge about bowing parameters associated with ΔE_V of quaternary $\text{AlInGaIn}/\text{GaN}$ hetero-junctions renders the same approach incapable of accurately evaluating the corresponding ΔE_C

TABLE III. Bandgap of binary III-Nitrides and ternary bowing parameters of bandgap.²¹

Parameter	Value (eV)
$E_G(\text{GaN})$	3.45
$E_G(\text{AlN})$	6.21
$E_G(\text{InN})$	0.68
b_{EG}^{AlGaIn}	0.9
b_{EG}^{InGaIn}	1.72
b_{EG}^{AlInIn}	6.43
	$1 + 1.21x^2$

values. Taking into account that throughout our current study In mole-fraction has to be smaller than that of Al (i.e., in order to keep the bandgap of AlInGaN barrier larger than the bandgap of GaN), in this case, the $\Delta E_C/\Delta E_V$ ratio can be assumed as 70:30, similar to the value that is usually used for AlGaIn/GaN hetero-structures.^{19,28}

C. Schottky barrier height

In this work, the Schottky barrier height is calculated assuming a Ni metal gate in contact with AlInGaN. Considering the Schottky barrier lowering, the barrier height is calculated according to

$$q\phi_B(V_{GS}) = q\phi_{m(Ni)} - q\chi_{AlInGaN} - \sqrt{\frac{q^3 E(V_{GS})}{4\pi\epsilon_{AlInGaN}}}, \quad (5)$$

where q is the unit charge, $q\phi_{m(Ni)}$ is the work-function of Ni, $q\chi_{AlInGaN}$ is the electron-affinity of AlInGaN, $\epsilon_{AlInGaN}$ is the dielectric constant of AlInGaN, V_{GS} is the gate-source voltage, and $E(V_{GS})$ is the electric field across the barrier-layer. The electron-affinity of the quaternary AlInGaN can be estimated applying Vegard's law.¹⁹ The expected uncertainty from this operation is intensified especially in case of high In mole fractions. This is since InN's electron-affinity can be determined with less precision compared to that of AlN and GaN.²⁹ As previously noticed, In mole fraction of AlInGaN barriers in the current study has to be small to guarantee the larger bandgap of AlInGaN barrier with respect to GaN. Hence, applying Vegard's law for calculation of electron-affinity in quaternary AlInGaN is deemed acceptable.

Since in the polar III-nitride system the polarization effect plays a dominant role in inducing the electric field across the barrier-layer, it is reasonable to assume a triangular potential barrier formed across this layer. As a result, the electric field across the barrier layer $E(V_{GS})$ based on^{28,30} is given by

$$E(V_{GS}) = \frac{(q\phi_B - qV_{GS}) + E_F - \Delta E_C}{qd_{AlInGaN}}, \quad (6)$$

where E_F is the fermi level and $d_{AlInGaN}$ is the thickness of the barrier-layer.

The 2DEG characteristics including 2DEG concentration (n_s), first and second subband energy levels (E_0 and E_1), and the position of fermi energy level are evaluated according to the procedure presented in Fig. 2. The calculation procedure starts by assuming an initial position for the fermi level (i.e., the lower edge of the conduction band of GaN at the hetero-interface). Using Eqs. (5) and (6), ϕ_B and E , which are mutually dependent, are calculated using an iterative approach. 2DEG concentration can be calculated in two ways. First, from the Gauss' law at hetero-interface

$$n_s = \frac{\sigma - \epsilon_{AlInGaN}E}{q}. \quad (7)$$

Second, in terms of the density of states function of the first and second subbands

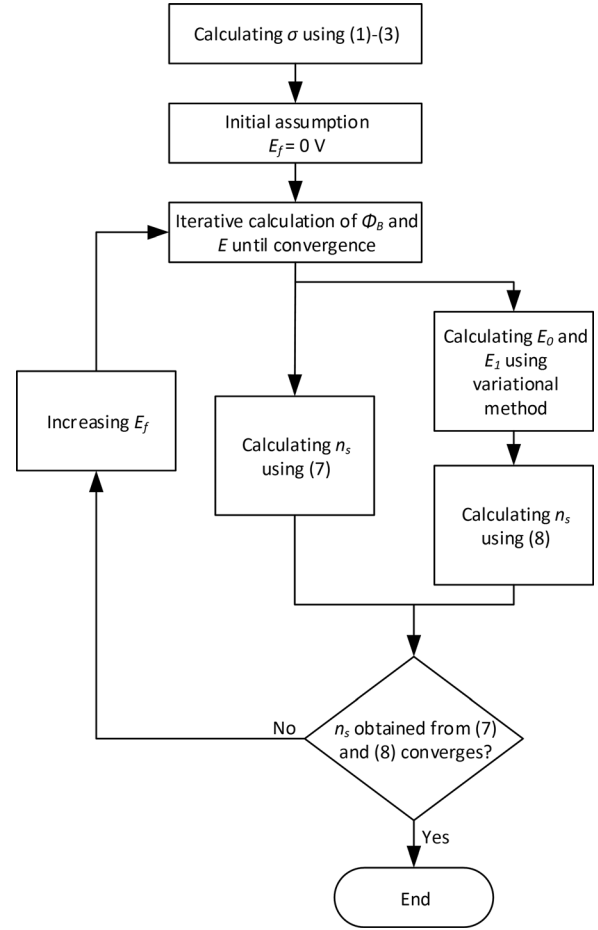


FIG. 2. Flowchart of the procedure for evaluation of 2DEG characteristics.

$$n_s = D_S \frac{kT}{q} \left\{ \ln \left[1 + \exp \left(\frac{E_f - E_0}{kT} \right) \right] + \ln \left[1 + \exp \left(\frac{E_f - E_1}{kT} \right) \right] \right\}, \quad (8)$$

in which D_S is two-dimensional density of states, k is the Boltzmann constant, and T is the temperature in kelvin. According to Ref. 18, E_0 and E_1 can be calculated through minimization of the total energy per electron using variational method as a function of E . In an iterative approach, E_f is gradually increased until the values obtained from Eqs. (7) and (8) converge with the relative error of less than 0.1%. For calculating the threshold voltage, n_s is considered as zero, and Eqs. (6)–(8) are re-evaluated to find the corresponding V_{GS} , which makes n_s equal to zero using the similar procedure.

III. RESULTS AND DISCUSSION

The accuracy of the model has been validated versus the 2DEG concentrations of the experimentally analyzed quaternary polar III-nitride samples reported in different studies. Employing a Ni Schottky contact, Table IV compares the calculated values of the 2DEG characteristics with published experimental data. The acceptable overall match between measurements and calculations is a testimony to the accuracy

TABLE IV. Simulation results of the physics-based model for the 2DEG characteristics of AlInGaN/GaN hetero-junctions previously reported in the literature. All of the devices are assumed to use a Ni gate.

Metal mole-fraction			Current study simulation					Experimental results			
Al	In	Ga	$d_{AlInGaN}$ (nm)	ϕ_B (V)	n_s (cm ⁻²)	σ (C/m ²)	V_T (V)	n_s (cm ⁻²)	V_T (V)	Error for n_s (%)	Ref.
0.74	0.16	0.1	12.5	2.21	2.02×10^{13}	0.0324	-4.9	1.81×10^{13}	-5.2	+11.60	13,31
0.7	0.15	0.15	11.8	2.14	1.53×10^{13}	0.037	-3.54	1.61×10^{13}	-4.5	-4.97	13,31
0.66	0.14	0.2	10.3	2.07	1.32×10^{13}	0.034	-2.71	1.52×10^{13}	-3.8	-13.16	13,31
0.48	0.17	0.35	8	1.68	1.58×10^{12}	0.018	-0.23	1.80×10^{12a}	0.56	—	17
0.11	0.02	0.87	8	1.09	— ^b	0.0047	0.63	8.00×10^{11}	0.2	—	17
0.16	0.02	0.82	20	1.19	2.19×10^{12}	0.0075	-9.17	1.80×10^{12}	— ^c	+21.67	32
0.34	0.03	0.63	20	1.54	8.37×10^{13}	0.0185	-3.46	1.13×10^{13}	— ^c	+25.93	32
0.52	0.03	0.45	20	1.90	1.70×10^{13}	0.0332	-6.99	2.29×10^{13}	— ^c	-25.76	32
0.72	0.14	0.14	5.6	2.19	1.15×10^{13}	0.0394	-1.38	1.13×10^{13}	— ^c	+1.77	33
0.73	0.11	0.16	5.3	2.24	1.40×10^{13}	0.0439	-1.63	1.36×10^{13}	— ^c	+2.94	33
0.73	0.11	0.16	15	2.24	2.14×10^{13}	0.0439	-6.33	2.14×10^{13}	— ^c	0.00	33
0.75	0.07	0.18	4.4	2.32	1.72×10^{13}	0.0512	-1.76	1.42×10^{13}	— ^c	+21.13	33
0.75	0.07	0.18	4.8	2.32	1.80×10^{13}	0.0512	-1.98	1.96×10^{13}	— ^c	-8.16	33
0.75	0.07	0.18	6.8	2.32	2.10×10^{13}	0.0512	-3.11	2.37×10^{13}	— ^c	-11.39	33

^aThe reported value is corresponding to the ungated region, hence no comparison is made to the theoretically evaluated value.

^bThis is a normally off device, thus, at $V_{GS} = 0$ V, 2DEG is already depleted and there is no quantum well. As a result, variational method cannot be used for evaluation of n_s , n_s would be almost equal to the background doping.

^cNo value has been reported.

of the model. Hence, in case of the samples for which the experimental results are not available, the current study can assist in forecasting the 2DEG characteristics.

Figure 3 illustrates the calculated conduction band edge diagrams of metal-face polar $\text{Al}_{0.3}\text{Ga}_{0.7}\text{N}/\text{GaN}$ and $\text{Al}_{0.3}\text{In}_{0.1}\text{Ga}_{0.6}\text{N}/\text{GaN}$ hetero-junctions of 20 nm thick barrier. As can be observed from this figure, for the latter set of mole-fractions (i.e., $x = 0.3$ and $y = 0.1$), a pronounced reduction of the polarization effect prevents the quantum-well at the hetero-interface from attracting enough carriers to form the 2DEG. For a constant Al mole-fraction, as In mole-fraction increases, the tensile strain in the barrier-layer decreases and eventually turns into a compressive strain (hence changing the direction of the piezoelectric polarization in the over-layer), while spontaneous polarization remains nearly constant. This is since the Al mole-fraction has not changed. As a result, total polarization is

reduced. In an AlInGaN/GaN HFET, reducing the polarization will lead to lower 2DEG carrier density and increase in the on-resistance of the device. Accordingly, it causes the threshold voltage to shift in the positive direction thereby producing a normally off device. Figure 4 presents the variation of threshold voltage of gated AlInGaN/GaN hetero-junctions versus the In mole-fraction for three different values of Al mole-fraction. Replacing Ga atoms with In (i.e., increasing In mole-fraction while Al mole-fraction remains constant) or Al atoms with In (i.e., increasing In mole-fraction while decreasing Al mole-fraction) can both increase the threshold voltage.

Variations of 2DEG concentration and threshold voltage of AlInGaN/GaN HFETs as functions of In mole-fraction and barrier thickness are illustrated in Fig. 5. Considering the variation of both the spontaneous and the piezoelectric polarizations, total polarization effect decreases with increasing In mole-fraction. This in turn reduces the density of the

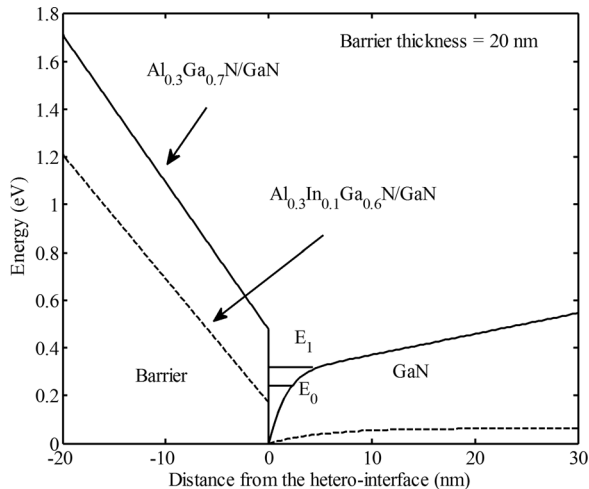


FIG. 3. Conduction band edge diagrams of $\text{Al}_{0.3}\text{Ga}_{0.7}\text{N}/\text{GaN}$ (full line) and $\text{Al}_{0.3}\text{In}_{0.1}\text{Ga}_{0.6}\text{N}/\text{GaN}$ (dashed line) hetero-junctions.

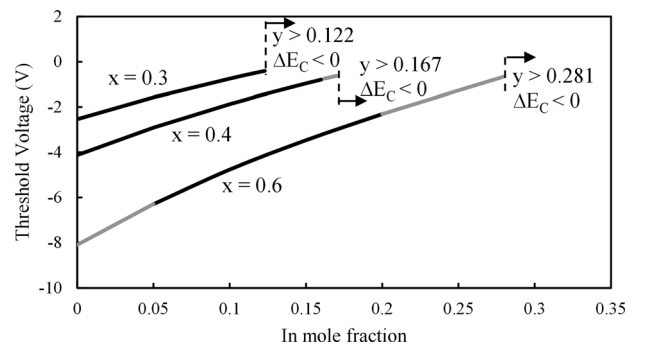


FIG. 4. Simulation results presenting the variation trend of threshold voltage of gated AlInGaN/GaN hetero-junctions (for Al mole-fractions of 0.3, 0.4, and 0.6) with the same barrier thickness of 20 nm versus In mole-fraction. The gray portions of each characteristic highlight the In mole-fractions, which render the 20 nm thickness of the barrier in excess of the strain-defined critical thickness. The limit of In mole fraction beyond which ΔE_C becomes negative is also indicated on each curve.

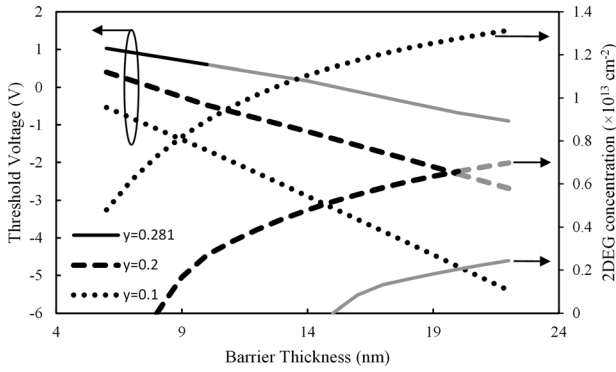


FIG. 5. Simulation results illustrating the 2DEG concentration and threshold voltage of AlInGaN/GaN HFETs versus barrier thickness for Al mole-fraction of 0.6 and three different In mole-fractions of 0.1, 0.2, and 0.281. The 2DEG concentrations are presented for $V_{GS} = 0$ V. In $Al_{0.6}In_{0.281}Ga_{0.119}N/GaN$ and $Al_{0.6}In_{0.2}Ga_{0.2}N/GaN$ HFET when the barrier is thinner than 15 and 8 nm, respectively, the 2DEG is completely depleted. The gray portions of each characteristic highlight the barrier thicknesses that are in excess of the strain-defined critical thickness. For Al mole fraction of 0.6. In mole fraction of 0.281 is the upper limit beyond which ΔE_C becomes negative.

polarization-induced charges at the hetero-interface. The depleting effect of the Schottky barrier is also observed to result in lower electron concentration, and the positive shift in threshold voltage, when the barrier becomes thinner. It is worth mentioning that the detrimental effect of crack formation in the barrier-layer at thicknesses beyond the critical thickness is not included in the theoretical evaluation.

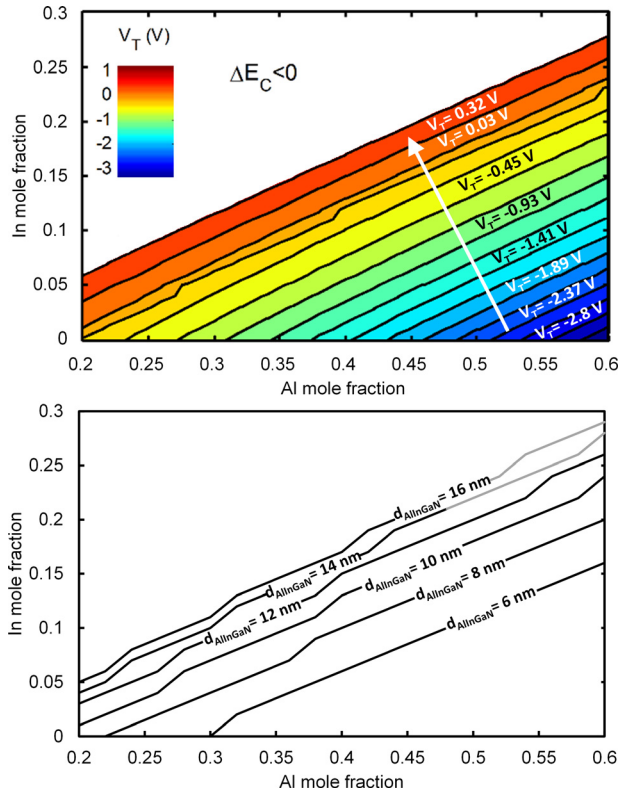


FIG. 6. (a) Simulation results presenting contours of threshold voltage of gated AlInGaN/GaN HFETs for different values of Al and In mole fractions. The barrier thickness is 10 nm. (b) Contours of $V_T = 0$ V for different values of barrier thickness. In (b), the gray portions of each characteristic highlight the barrier thicknesses that are in excess of the strain-defined critical thickness at the corresponding metal mole-fractions.

According to these observations, in order to realize a normally off HFET, higher In mole-fraction and thinner barrier should be employed simultaneously. Figure 6(a) through depicting contours of threshold voltage for different metal mole-fractions highlights the applicable compositional window for the realization of normally off characteristic when the barrier thickness is 10 nm. Figure 6(b) illustrates the contours of $V_T = 0$ V for different values of barrier thickness. Based on this figure, for the devices employing thinner barriers, threshold voltage of zero can be realized at lower values of In mole-fraction. Similar threshold voltages for the devices with almost equal ratio of Al and In mole-fractions can be interpreted from both panels of Fig. 6.

Figure 7 presents variations of the subband energy levels and the fermi level as functions of y , for different values of x . According to the simulation results, increasing y exhibits the same effect as decreasing x , which causes the positions of the two subband energy levels to converge while the fermi energy levels decrease. A possible explanation for these observations can be found in reduction of the polarization effect caused by In incorporation, which results in weaker carrier confinement. In this condition, the hetero-interface quantum well gets wider and shallower. Although 2DEG subband levels get closer, as the relative position of fermi level with respect to E_0 and E_1 drops, the probability of occupation of free states in these subbands decreases. As a result, 2DEG can be depleted more easily yielding a normally off device.

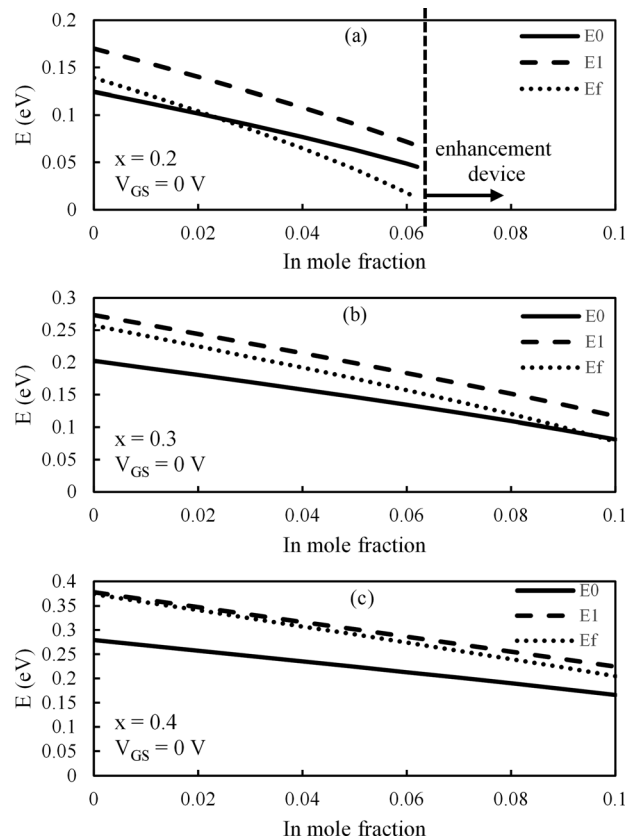


FIG. 7. Illustration of the first and second subband energy levels (i.e., E_0 and E_1) and fermi energy level (i.e., E_F) as functions of In mole-fraction, for different values of Al mole-fractions when $V_{GS} = 0$ V. The barrier thickness is 20 nm. The reference for all energy levels is the energy level of conduction band edge at hetero-interface.

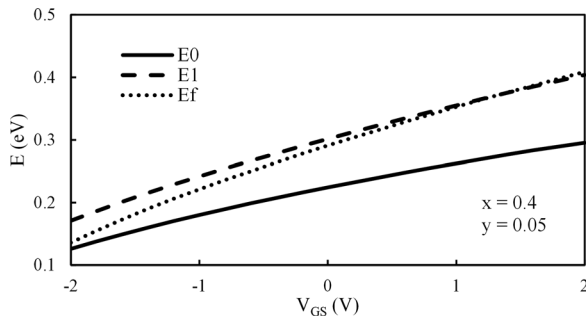


FIG. 8. Illustration of the first and second subband energy levels (i.e., E_0 and E_1) and fermi energy level (i.e., E_f) as functions of V_{GS} for $\text{Al}_{0.4}\text{In}_{0.05}\text{Ga}_{0.55}\text{N}/\text{GaN}$ HFET. The reference for all energy levels is the energy level of conduction band edge at hetero-interface. The barrier thickness is 20 nm.

Initial inspection of Fig. 7 also reveals that increase in y results in the fermi energy level lying further from the second subband energy level. Therefore, it might be deduced that consideration of the second subband energy level is in vain. However, it should be noted that the results presented in this figure are based on the hetero-junctions with $V_{GS} = 0$ V, whereas the hetero-junctions with higher In mole-fractions normally operate at higher V_{GS} values. For clarifying the effect of V_{GS} , Fig. 8 provides variations of the subband energy levels and the fermi level as functions of V_{GS} for an $\text{Al}_{0.4}\text{In}_{0.05}\text{Ga}_{0.55}\text{N}/\text{GaN}$ HFET. According to the simulation results, increasing the gate-source voltage imposes an effect opposite to that of higher In mole-fraction on the position of subband energy levels versus the fermi level. As a result, as in ternary AlGaIn/GaN hetero-junctions for quaternary hetero-junctions, it would not be reasonable to ignore the presence of the second subband energy level.

IV. CONCLUSION

The 2DEG characteristics of $\text{AlInGaIn}/\text{GaN}$ hetero-junctions are theoretically modeled using the variational method. It is confirmed that the threshold voltage of a quaternary GaN-based hetero-junction can be increased to values above zero by engineering both the spontaneous and the piezoelectric polarization. Furthermore, this study reveals that in obtaining this end-goal, reducing the polarization through attempting a polarization-matched hetero-structure is not capable of offering the chance of channel formation on the GaN side of the hetero-junction. Hence, a coordinated use of relatively thin barrier (i.e., to enhance Schottky depletion) and strain engineering via incorporation of In in the barrier is needed to warrant a positive threshold voltage. The calculated 2DEG concentrations based on the present theoretical evaluation agree with the experimental values reported in the literature. Results show that the first and second subbands become closer and the position of fermi level reduces as In mole-fraction increases or Al mole-fraction decreases.

ACKNOWLEDGMENTS

The authors would also like to thank the support of the Natural Sciences and Engineering Research Council of Canada (NSERC) Discovery Grant program.

- ¹U. K. Mishra, P. Parikh, and Y.-F. Wu, *Proc. IEEE* **90**, 1022 (2002).
- ²S. Keller, Y.-F. Wu, G. Parish, N. Ziang, J. J. Xu, B. P. Keller, S. P. DenBaars, and U. K. Mishra, *IEEE Trans. Electron Devices* **48**, 552 (2001).
- ³Y.-F. Wu, M. Moore, A. Saxler, T. Wisleder, and P. Parikh, "40-W/mm double field-plated GaN HEMTs," in *64th Device Research Conference, State College, PA, USA* (IEEE, June 2006), pp. 151–152.
- ⁴T. Palacios, A. Chakraborty, S. Rajan, C. Poblenz, S. Keller, S. P. DenBaars, J. S. Speck, and U. K. Mishra, *IEEE Electron Device Lett.* **26**, 781 (2005).
- ⁵J. W. Chung, W. E. Hoke, E. M. Chumbes, and T. Palacios, *IEEE Electron Device Lett.* **31**, 195 (2010).
- ⁶P. Srivastava, J. Das, D. Visalli, M. Van Hove, P. E. Malinowski, D. Marcon, S. Lenci, K. Geens, K. Cheng, and M. Leys, *IEEE Electron Device Lett.* **32**, 30 (2011).
- ⁷M. Nakatsugawa, Y. Yamaguchi, and M. Muraguchi, *IEEE Trans. Microw. Theory Tech.* **43**, 1745 (1995).
- ⁸Y. Cai, Y. Zhou, K. Chen, and K. Lau, *IEEE Electron Device Lett.* **26**, 435 (2005).
- ⁹R. Chu, Z. Chen, S. P. DenBaars, and U. K. Mishra, *IEEE Electron Device Lett.* **29**, 1184 (2008).
- ¹⁰K. Ohi and T. Hashizume, *Jpn. J. Appl. Phys., Part 1* **8**, 081002-1 (2009).
- ¹¹P. Valizadeh and B. AlOtaibi, *IEEE Trans. Electron Devices* **58**, 1404 (2011).
- ¹²H. Hahn, B. Reuters, A. Wille, N. Ketteniss, F. Benkhelifa, O. Ambacher, H. Kalisch, and A. Vescan, *Semicond. Sci. Technol.* **27**, 1 (2012).
- ¹³N. Ketteniss, L. Rahimzadeh Khoshroo, M. Eickelkamp, M. Heuken, H. Kalisch, R. H. Jansen, and A. Vescan, *Semicond. Sci. Technol.* **25**, 075013 (2010).
- ¹⁴C. B. Soh, S. J. Chua, S. Tripathy, S. Y. Chow, D. Z. Chi, and W. Liu, *J. Appl. Phys.* **98**, 103704-1 (2005).
- ¹⁵Y. Liu, T. Egawa, and H. Jiang, *Electron. Lett.* **42**, 884 (2006).
- ¹⁶B. Reuters, H. Hahn, A. Pooth, B. Hollander, U. Breuer, M. Heuken, H. Kalisch, and A. Vescan, *J. Phys.D: Appl. Phys.* **47**, 175103 (2014).
- ¹⁷B. Reuters, A. Wille, N. Ketteniss, H. Hahn, B. Holländer, M. Heuken, H. Kalisch, and A. Vescan, *J. Electron. Mater.* **42**, 826 (2013).
- ¹⁸F. Manouchehri, P. Valizadeh, and M. Z. Kabir, *J. Vac. Sci. Technol. A* **32**, 021104-1 (2014).
- ¹⁹J. Piprek, *Nitride Semiconductor Devices* (Wiley-VCH, Weinheim, 2007).
- ²⁰M. A. Laurent, G. Gupta, S. Wienecke, A. A. Muqtadir, S. Keller, S. P. DenBaars, and U. K. Mishra, *J. Appl. Phys.* **116**, 183704 (2014).
- ²¹E. Sakalauskas, B. Reuters, L. Rahimzadeh Khoshroo, H. Kalisch, M. Heuken, A. Vescan, M. Röppischer, C. Cobet, G. Gobsch, and R. Goldhahn, *J. Appl. Phys.* **110**, 013102 (2011).
- ²²S. H. Park, Y. T. Moon, D. S. Han, J. S. Park, M. S. Oh, and D. Ahn, *Appl. Phys. Lett.* **99**, 181101 (2011).
- ²³I. Gorczyca, T. Suski, N. E. Christensen, and A. Svane, *Appl. Phys. Lett.* **24**, 241905 (2011).
- ²⁴D. Jena, J. Simon, A. K. Wang, Y. Cao, K. Goodman, J. Verma, S. Ganguly, G. Li, K. Karda, V. Protasenko, C. Lian, T. Kosel, P. Fay, and H. Xing, *Phys. Status Solidi A* **208**, 1511 (2011).
- ²⁵G. A. Martin, A. Botchkarev, A. Agarwal, A. Rockett, and H. Morkoç, *Appl. Phys. Lett.* **68**, 2541 (1996).
- ²⁶H. Morkoç, *Handbook of Nitride Semiconductors and Devices* (Wiley-VCH, Berlin, 2008), Vol. 3.
- ²⁷S. Satpathy, Z. S. Popovic, and W. C. Mitchel, *J. Appl. Phys.* **95**, 5597 (2004).
- ²⁸O. Ambacher, B. Foutz, J. Smart, J. R. Shealy, N. G. Weimann, K. Chu, M. Murphy, A. J. Sierakowski, W. J. Schaff, L. F. Eastman, R. Dimitrov, A. Mitchell, and M. Stutzmann, *J. Appl. Phys.* **87**, 334 (2000).
- ²⁹T. D. Veal, C. F. McConville, and W. J. Schaff, *Indium Nitride and Related Alloys* (CRC Press, 2010), p. 381.
- ³⁰S. Karmalkar, D. M. Sathaiya, and M. S. Shur, *Appl. Phys. Lett.* **82**, 3976 (2003).
- ³¹L. Rahimzadeh Khoshroo, N. Ketteniss, C. Mauder, H. Behmenburg, J. F. Woitok, I. Booker, J. Gruis, M. Heuken, A. Vescan, H. Kalisch, and R. H. Jansen, *Phys. Status Solidi* **7**, 2001 (2010).
- ³²B. Reuters, A. Wille, B. Holländer, E. Sakalauskas, N. Ketteniss, C. Mauder, R. Goldhahn, M. Heuken, H. Kalisch, and A. Vescan, *J. Electron. Mater.* **41**, 905 (2012).
- ³³X. Gao, M. Pan, D. Goroka, M. Oliver, M. Schuette, A. Ketterson, and P. Saunier, *Phys. Status Solidi* **11**, 495 (2014).